Physics of Plasmas

Kinematics of femtosecond laser-generated plasma expansion: Determination of sub-micron density gradient and collisionality evolution of over-critical laser plasmas

Cite as: Phys. Plasmas **28**, 093109 (2021); https://doi.org/10.1063/5.0038549
Submitted: 24 November 2020 • Accepted: 29 July 2021 • Published Online: 23 September 2021

G. G. Scott, G. F. H. Indorf, M. A. Ennen, et al.

Physics of Plasmas ARTICLE scitation.org/journal/php

Kinematics of femtosecond laser-generated plasma expansion: Determination of sub-micron density gradient and collisionality evolution of over-critical laser plasmas

Cite as: Phys. Plasmas **28**, 093109 (2021); doi: 10.1063/5.0038549
Submitted: 24 November 2020 · Accepted: 29 July 2021 ·
Published Online: 23 September 2021

G. G. Scott,[1,2,a)] G. F. H. Indorf,[2,3] M. A. Ennen,[3] P. Forestier-Colleoni,[4] S. J. Hawkes,[2] L. Scaife,[2] M. Sedov,[5] D. R. Symes,[2] C. Thornton,[2] F. Beg,[4] T. Ma,[1] P. McKenna,[6] A. A. Andreev,[3,7,8,9] U. Teubner,[3,10] and D. Neely[2,6,b)]

AFFILIATIONS

[1]Lawrence Livermore National Laboratory, Livermore, California 94550, USA
[2]Central Laser Facility, STFC Rutherford Appleton Laboratory, Didcot OX11 0QX, United Kingdom
[3]Institut für Laser und Optik, Hochschule Emden/Leer-University of Applied Sciences, Emden 26723, Germany
[4]Center for Energy Research, University of California San Diego, La Jolla, California 92093, USA
[5]Joint Institute for High Temperatures of the Russian Academy of Sciences, Moscow 125412, Russian Federation
[6]Department of Physics SUPA, University of Strathclyde, Glasgow G4 0NG, United Kingdom
[7]Saint-Petersburg State University, St. Petersburg 199034, Russian Federation
[8]ELI-ALPS, Szeged H-6720, Hungary
[9]Max Born Institute, Berlin 12489, Germany
[10]Institut für Physik, Carl von Ossietzky Universität, Oldenburg 26111, Germany

[a)]**Author to whom correspondence should be addressed:** scott110@llnl.gov
[b)]Deceased.

ABSTRACT

An optical diagnostic based on resonant absorption of laser light in a plasma is introduced and is used for the determination of density scale lengths in the range of 10 nm to $>1\,\mu$m at the critical surface of an overdense plasma. This diagnostic is also used to extract the plasma collisional frequency, allowing inference of the temporally evolving plasma composition on the tens of femtosecond timescale. This is found to be characterized by two eras: the early time and short scale length expansion ($L < 0.1\lambda$), where the interaction is highly collisional and target material dependent, followed by a period of material independent plasma expansion for longer scale lengths ($L > 0.1\lambda$); this is consistent with a hydrogen plasma decoupling from the bulk target material. Density gradients and plasma parameters on this scale are of importance to plasma mirror optical performance and comment is made on this theme.

I. INTRODUCTION

A renewed interest in the plasma mirror (PM)[1–3] is evident from a wealth of recent investigations emerging from the literature. These cover a range of topics including optical performance optimization;[4–7] high repetition rate designs of thin and ultrathin PMs,[8–11] which are suited to multistage wakefield acceleration for example;[12] focusing PMs,[13–15] which can be used as an active optical element, leading to focused intensity enhancement; PMs for secondary radiation source generation;[16–18] and a range of implementation studies.[7,19,20]

As the PM's repertoire evolves, the matter of their efficiency becomes increasingly important as they have traditionally been considered a lossy component with a reflectivity commonly measured to be around 70%. However, it was recently shown this can be significantly increased to 96%, when a 10^{15} W cm^{-2}, 1.054 μm, s-polarized

laser pulse interacted with a finite plasma density gradient of (0.1–0.3)λ on the surface.[4] To further investigate this efficiency control mechanism, we have devised a technique to experimentally determine the plasma sub-micron density scale length, collisionality, and temperature, such that they can be experimentally correlated with PM performance. Measuring sub-micron density gradients is a useful measurement to make in itself for diagnosing overdense laser-plasma interactions, as many phenomena have been shown to be sensitively dependent on the laser interaction with short density scale lengths, such as harmonic generation,[21–25] ion acceleration[26–28] from surface monolayers,[29,30] soft[31,32] or keV[33] x-ray generation, and instability growth.[34,35]

Experimental measurement of sub-micron density gradients using conventional techniques is challenging, as imaging or interferometry does not offer the necessary spatial resolution at optical wavelengths and strong refraction and bright, broadband self-emission in the vicinity of the critical density compounds this difficulty. However, when physical phenomena are markedly sensitive to variations of the scale length on this order, measurements of these phenomena and variations in them can be used as diagnostics of the scale length.[36–38] For the work in this manuscript, the technique of resonance absorption profile spectroscopy provides a means to determine such scale lengths,[39] and we introduce an optical variant of this technique. Since the efficiency of resonant absorption is inherently sensitive to density scale lengths on the order of the laser wavelength and optimal absorption occurs at a specific scale length for a given incidence angle, the scale length can be extracted by fitting experimental data to a theoretical model, as well as the collision frequency or electron temperature, which are notoriously difficult to estimate in the strongly coupled regime where the potential of the plasma exceeds the kinetic energy of the particles.

In Sec. II, we describe an analytic model of linearly polarized laser absorption by a plasma and benchmark it against previously published numerical and experimental results, before using it to extract information by fitting the model to the experimental results of this manuscript, described in Secs. III and IV. In Sec. VI, we will present some detailed discussion on the theme of the physics derived from this diagnostic and some possibilities for adapting the diagnostic for single-shot plasma evolution measurement, before discussing the implications of this work for PM optical performance optimization.

II. ANALYTIC MODEL—LASER ENERGY ABSORPTION IN SHORT DENSITY SCALE LENGTHS

A. Formulation for p-polarized interactions

In order to interpret our experimental results, we first develop an analytic model to describe p-polarized laser light absorption in short density plasma scale length plasmas, beginning by considering a plasma occupying a semi-infinite space ($x \geq 0$), with a linear electron density profile ($x \leq 0$):

$$\eta_e(x) = \frac{n_e(x)}{n_0} = \begin{cases} 1 & x \geq 0, \\ 1 + x/LN & -LN \leq x \leq 0, \end{cases} \tag{1}$$

where the scale length, L, describes the spatial scale over which the electron density, n_e, decreases. In the region where the plasma density is overcritical ($N = n_0/n_{cr} = \omega_{pe}^2/\omega^2 \geq 1$), the electromagnetic field (described in terms of E and $B = \mu H$) incident on the plasma at an angle, θ, is given by the following expressions:

$$\begin{gathered} E = (E_x, E_y, 0), \\ H = (0, 0, H), \\ E, H \sim \exp\left[-i\omega t + i\omega y \cdot \sin(\theta/c)\right]. \end{gathered} \tag{2}$$

The dielectric constant, ϵ, of the plasma can be written as

$$\epsilon = 1 - \frac{N\eta_e(x)}{[1 + i\beta_P N\eta_e(x)]}, \tag{3}$$

where $\beta = \nu_c/\omega$ is the electron collision frequency at the critical electron density normalized to the angular frequency of the electromagnetic radiation, ω. We consider the Helmholtz equation for the magnetic component:

$$\frac{d^2H}{dx^2} - \frac{1}{\epsilon}\left(\frac{d\epsilon}{dx}\right)\left(\frac{dH}{dx}\right) + \frac{\omega^2}{c^2}(\epsilon - \sin^2\theta) \cdot H = 0. \tag{4}$$

For long scale lengths ($L/\lambda > 1$), the dielectric constant is slowly varying on the scale of the laser wavelength and in this case, (4) can be solved within the WKB approximation,[42,43] and the laser absorption efficiency ($|E|^2$) by the plasma is given by

$$\eta_{WKB} = 1 - \exp\left(-\frac{8}{3}\beta_{WKB}\omega\frac{L}{c}\cos^3\theta\right). \tag{5}$$

In the case of short scale lengths ($L/\lambda < 1$), the WKB approximation fails and we therefore aim to develop a solution of (4) in the limit where the collision frequency is small, $\beta_P \ll 1$. A more detailed version of the following derivation is presented in the Appendix. Introducing a new variable, $\xi = x/L + N + 1$, and substituting (3) into (4), we obtain (6), where $\alpha = (\omega L/c)^2$ and $S = \sin^2\theta$:

$$\begin{aligned} \frac{d^2H}{d\xi^2} - \frac{dH/d\xi}{\xi - i\beta_P(1+\xi)][1 + i\beta_P(1+\xi)]} \\ - \alpha H\left[\frac{\xi - i\beta_P(1+\xi)}{(1 + i\beta_P(1+\xi)} + S\right] = 0. \end{aligned} \tag{6}$$

A solution of (6) can be found by making the assumption that $\alpha \ll 1$. It should be noted that one cannot expand H in terms of α directly in (6), since the last term, proportional to α, may become large at $\xi \to \infty$, so (6) is solved for the edge region ($\xi \cong 1$) and in the plasma bulk ($\xi \gg 1$) separately and then matching of the expansions is performed.

When the magnetic field, H, is known, the electrical component, E_y, and the absorption efficiency of the p-polarized light in the density scale length, η_P, are given by (7):[45]

$$\begin{gathered} E_y = i\epsilon^{-1}\alpha^{-1/2}dH/d\xi, \\ \eta_P = 1 - |(\zeta - \cos\theta)/(\zeta + \cos\theta)|^2, \end{gathered} \tag{7}$$

where $\zeta = (E_y/H)|_{\xi=1}$ is the surface impedance.

Considering the region, $1 \leq \xi \leq N + 1$, where the last term in Eq. (6) is small compared with the other terms. Setting $\alpha = 0$, we obtain a zeroth-order approximation to the edge solution, which is valid for all values of β_P:

$$\begin{aligned} H_0 = 2D\left[\frac{i}{\beta_P^2}\arctan[\beta_P(1+\xi)] - \frac{\xi(i+\beta_P)}{\beta_P}\right. \\ \left. + \frac{1}{2\beta_P^2}\ln\left[1 + \beta_P^2(1+\xi)^2\right]\right] + B, \end{aligned} \tag{8}$$

where D and B are undefined constants. Treating β_P^2 as a small parameter in the same way as α and substituting (9) into (6), the surface impedance is obtained in (10). Along with the terms in (A11), the absorbed energy fraction from the p-polarized interaction, η_P, can be obtained from (7).

$$H = H_0(\xi) + \alpha H_\alpha(\xi) + i\beta_P H_{\beta_P}(\xi) + \cdots, \tag{9}$$

$$\zeta = 2i\alpha^{-1/2}(D + \alpha D_1 + i\beta_P D_2)\cdot(D + B + \alpha(D_1 + B_1) + i\beta_P D_2)^{-1}, \tag{10}$$

where

$$D_1, D_2, B_1, B_2, q_0, \text{ and } q_1 \tag{11}$$

are constants to be defined by matching the edge and bulk solutions (see the Appendix). The capability of the matching procedure is provided by the assumption $\alpha \ll 1$, because in this case, the edge region can overlap the bulk one.

Relation (10) can be approximated by

$$\zeta \approx -1.38i\cdot\alpha^{1/6}[1 - \alpha^{1/3}S] + \pi\alpha^{1/2}S + 0.38\beta_P\alpha^{-1/6}, \tag{12}$$

where the real terms are responsible for resonant and collisional parts of the total absorption efficiency. The absence of the angular dependence in the last term of (12) implies the equality of collisional absorption efficiency for the s- and p-polarized waves in the considered approximation. We do not consider Brunel absorption mechanism[44] in our conditions because of its inefficiency at the laser intensities investigated in our experimental work.

Note, that for $L/\lambda \ll 1$, the laser wave penetrates well beyond the critical surface and the collision frequency is not defined by Spitzer theory. The p-polarization absorption efficiency has two limits: for $L/\lambda \gg 1$, $\eta_P \approx \eta_S \approx \eta_{WKB}$; and at the other limit, $L/\lambda \ll 1$, $\eta_{WKB} \to 0$, and the main contribution to the absorption is described by Eq. (7). Thus, in the intermediate region, one can match the solutions of Eqs. (5) and (7) by simple addition as in Eq. (13),

$$\eta_{P_{TOTAL}} = \eta_P + \eta_{WKB}. \tag{13}$$

The p-polarized wave absorption is therefore described by two different collisional frequencies. For short scale lengths, β_P is dictated by absorption in the overdense plasma with an efficiency, η_P, and for long scale lengths, β_P is dictated by β_{WKB} in the underdense plasma, with an efficiency, η_{WKB}. It is to be expected that as the scale length of the plasma gets longer the observed collisional frequency dictating the efficiency of p-polarized wave absorption, $\beta_{P_{OBS}}$, would be observed to evolve, owing to the changing absorption mechanism that dominates at a given density scale length range.

B. Formulation for s-polarized interactions

Considering s-polarized interactions with large scale length plasma, the WKB approximation has been shown to work well for describing the absorption of laser energy, whilst for small scale length plasmas the approximation formula given by Andreev *et al.*[47] is shown in (14):

$$\eta_S \approx C_p\beta_S^{0.7}\left(\frac{L}{\lambda}\right)^{-0.3}\left(\frac{n_e}{n_{cr}}\right)^{0.2}, \quad C_p \approx 0.07. \tag{14}$$

Therefore, by combining (5) and (14) we can retrieve a more general form of the absorption efficiency of s-polarized in a range of density scale lengths, by using (15):

$$\eta_{S_{TOTAL}} = \eta_S + \eta_{WKB}. \tag{15}$$

Unlike the p-polarized wave, both mechanisms by which the s-polarized wave is absorbed are here described by the same collisional frequency, $\beta_S = \beta_{WKB}$. It would be expected that for all scale lengths, the observed quantity, $\beta_{S_{OBS}}$, would remain constant.

C. Validation

In order to validate the analytic model, Eq. (7) is evaluated using the terms in Eqs. (10) and (A10) are compared to the data from Figs. 4 (0° incidence) and 5 (45° incidence) of Kieffer *et al.*,[46] where in their work, the authors numerically solved Eq. (4) for exponential profiles.

The comparison is shown in Fig. 1(a), and good agreement is obtained between the numerical and analytic models for normal and

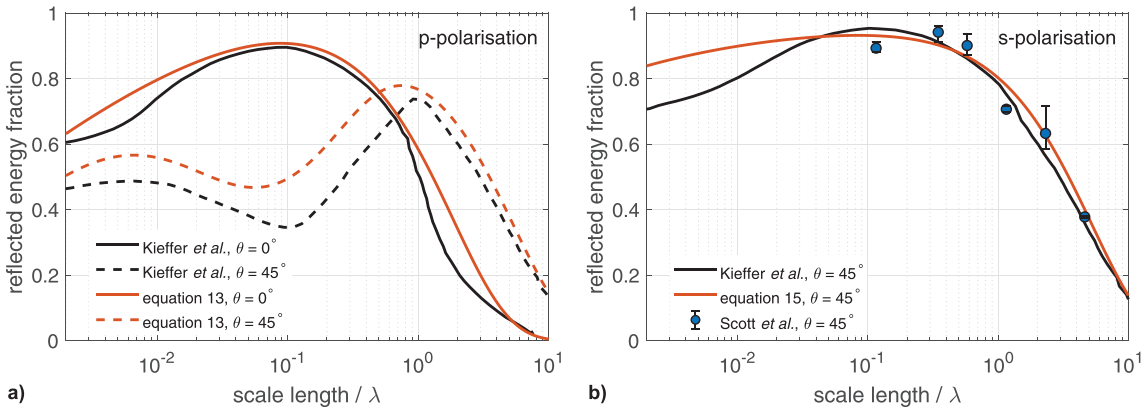

FIG. 1. The analytic model benchmarked against numerical data by Kieffer *et al.*[46] for (a) p-polarized and (b) s-polarized interactions at various angles of incidence, where $\beta = 0.04$. (a) Kieffer *et al.*'s data at 0° and 45° interactions are extracted from their Figs. 4 and 5, respectively. (b) Kieffer *et al.*'s data are extracted from their Fig. 6(b). Experimental data from Scott *et al.*[4] are also shown.

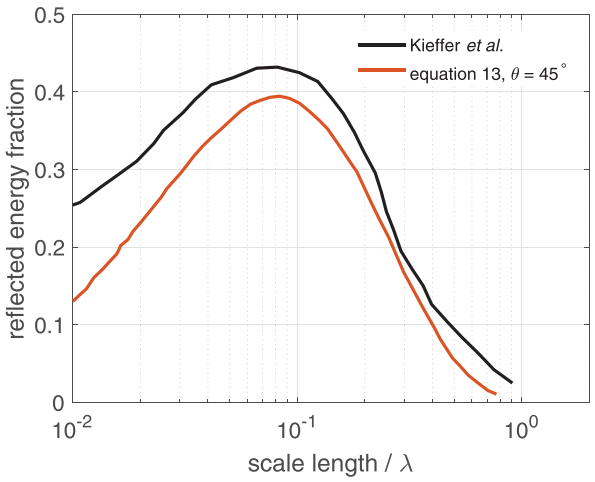

FIG. 2. The analytic model benchmarked against numerical data from Fig. 4 of Kieffer *et al.*[46] for p-polarized interactions at 45° incidence and a higher collision frequency $\beta_P = 0.32$.

45° incidence angles, both in terms of the qualitative shapes of the curves and the absorption efficiency that they predict. The comparison of the analytic model equation (15) for absorption of s-polarized laser pulses with the numerical model of Kieffer *et al.* is shown in Fig. 1(b).

In deriving the analytic model, a linear density profile was assumed, whereas in experiment and simulation, an exponential profile is typically observed and we consider the impact of this on the analytic model results. We note that the results of the analytic model are compared with a numerical solution using an exponential density profile and the good agreement obtained shows that our model is valid under these conditions.

Second, the analytic model is derived under the assumption that $\beta_P \ll 1$. In Fig. 2, we compare numerical calculations from Kieffer *et al.*[46] with $\beta_P = 0.32$. This shows that for $L/\lambda > 4 \times 10^{-2}$, the analytic model agrees with the calculation for high collision frequencies to 15%, and for $L/\lambda < 4 \times 10^{-2}$, it agrees to 26%. In Secs. IV and V interpretation of experimental data should therefore be considered to be valid when this condition is found to be true.

The good degree of agreement gives us confidence that the analytic model has captured the key physics that describes the mechanism of absorption of laser energy in plasma density scale lengths and that robust conclusions about the plasma parameters can be obtained by fitting the model to experimental data.

III. EXPERIMENTAL METHODS

The experiment was carried out at the Central Laser Facility using the Gemini TA2 experimental area. The laser is a Titanium:Sapphire system, which produced pulses of 60 fs duration for this experiment at a central wavelength of 800 nm with up to 500 mJ of energy on target. The laser intensity contrast, being the ratio of instantaneous intensity to that of the main pulse, was measured to be $>10^{-10}$, 10^{-7}, and 10^{-4} at 50, 5, and 0.5 ps prior to the main pulse, respectively.

A prepulse generator was installed in the beamline at the postamplification and pre-compressor stage, and a schematic of this is shown in Fig. 3. Using a calorimeter, we measured the energy partition between the beams to be 1:10 (prepulse to main pulse) and typically (19:190) mJ was delivered to the target chamber for results presented in this study. The collinear beams were temporally synchronized to within the laser pulse duration by varying the position of the delay stage until interference fringes were observed on a post-compression near field diagnostic.

In the interaction chamber, the common polarization of the pulses was controlled by a half-wave plate and focused onto the target with a gold-coated off-axis parabola with a focal length of 50.8 mm and aperture of 55 mm at a central angle of incidence of 48°.

The PM target was reproducibly positioned in the focal plane using a collinear internal CW laser and retro imaging system,[40] to

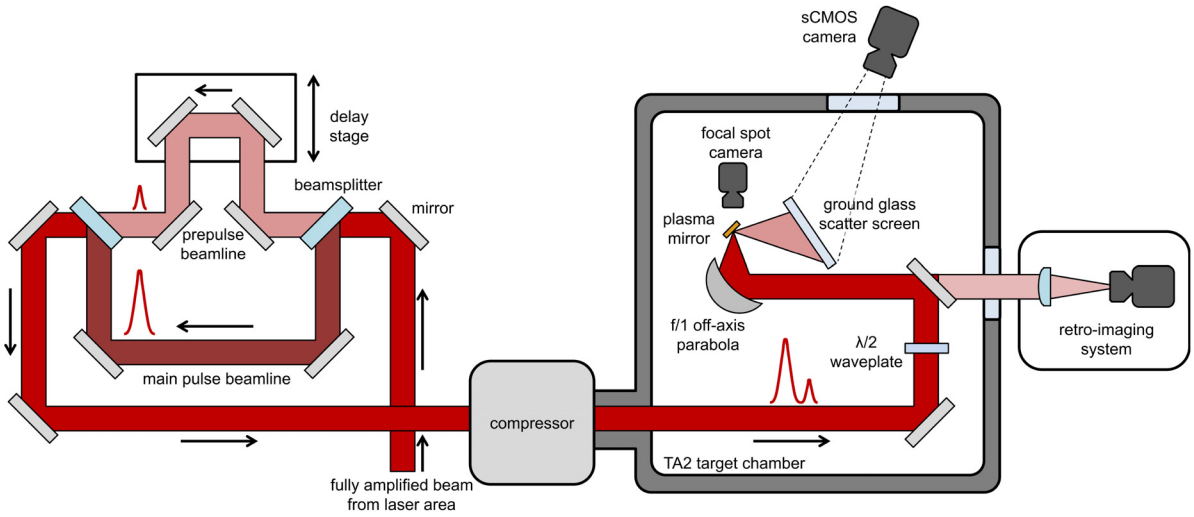

FIG. 3. Left: the pre-compressor, prepulse generator. Right: the experimental setup in the TA2 vacuum chamber.

within an error comparable to the Rayleigh range of the off-axis parabola, and was typically positioned at a defocused position of 200 μm. The intensity on target was then varied by controlling the incoming laser energy, which was monitored shot to shot by a pre-compressor near-field diagnostic.

After interaction, the reflected beam is directed toward a ground glass scatter screen, from which the reflected near field is imaged by a high-dynamic-range ANDOR Neo 5.5 sCMOS camera. With the plasma reflectivity known to have an angular dependence, only the energy content of the central $\pm 2.5^\circ$ portion of the beam is considered in the analysis presented here.

IV. EXPERIMENTAL RESULTS

A. Single pulse interactions

Prior to investigating the interaction of the laser with a density scale length, the experimental setup was used to characterize the intensity dependent, integrated reflectivity of a single laser pulse from an interaction with an uncoated BK7 glass substrate. Many experiments have been conducted using similar parameter ranges, and these shots therefore serve to benchmark the experimental setup.

The results of this characterization study are presented in Fig. 4, for both s- and p-polarization interactions, and good agreement is obtained between the results here and those published elsewhere for s-polarized pulses with these wavelengths and pulse duration.[1,41]

B. Interactions with a prepulse formed plasma scale length

On introduction of the controlled prepulse, the reflectivity of the plasma as a function of interpulse time delay was investigated for multiple materials under the same irradiation conditions. BK7 glass (SiO_2), sapphire (Al_2O_3), copper, and gold substrates were chosen as dielectrics are common PM substrate materials, and gold has a significantly different charge and mass from these, enabling any dependence of the interaction on the substrate material to be discernible in the experimental results.

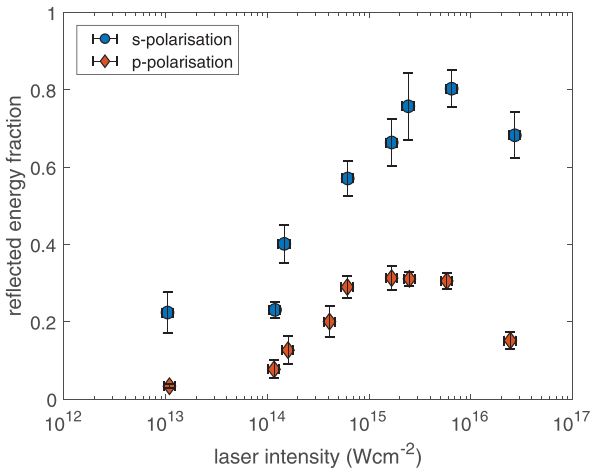

FIG. 4. Reflectivity measurements from a series of single pulse interactions by varying intensity and polarization with uncoated BK7 glass.

Figure 5 shows the experimental results of the main pulse reflected energy fraction obtained at various interpulse time delays, where the plasma expansion is initiated by a prepulse with an intensity of 2×10^{14} W cm^{-2}, and the main pulse therefore probed the expansion with ten times that intensity.

1. Temporally evolving scale length

The main pulse reflected energy fraction behavior from s-polarized interactions is consistent with that obtained in the past,[4] where a peak in the plasma reflectivity is observed at an optimal scale length and interpulse time delay of a few picoseconds.

Data from interactions with an s-polarized laser pulse are well reproduced by the analytic model described by Eq. (15), where the scale length of the model is fitted to the experimental data by assuming an isothermal plasma expansion, governed by the sound speed c_s, over time by the relation, $L = c_s t$. Performing a least squares fit of the model to the experimental data yields a sound speed of $c_s = 24$ nm ps^{-1} and a collision frequency of $\beta_{S_{OBS}} = 0.054$.

This allows the electron temperature of the plasma to be calculated using the straightforward relationship in Eq. (16) and is estimated to be $\approx$6 eV by assuming that protons are the dominant ion species in the expansion. In the coming paragraphs, we will present independent pieces of evidence for this assumption.

$$c_s = \left(\frac{Z^* k_B T_e}{m_i}\right)^{\frac{1}{2}}, \quad T_e = \frac{m_i c_s^2}{Z^* k_B}. \tag{16}$$

The absorption of the p-polarized pulse is also shown for all materials investigated in Fig. 5, and qualitatively, the experimental

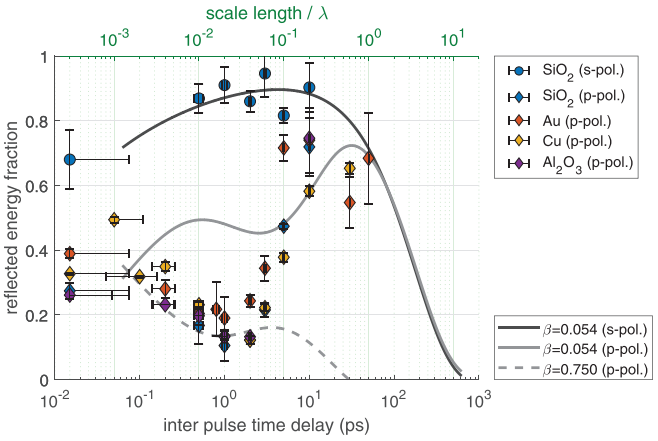

FIG. 5. Experimentally measured main pulse reflected energy fraction (data points) from double pulse interactions, where the experimentally controlled delay between the pulses is given on the lower x-axis. The polarization dependence was investigated using BK7 glass (SiO_2), and the material dependence was investigated using multiple target materials. Curves are obtained from fitting the analytic model, using Eq. (15) to model s-polarization and Eqs. (10) and (A10) for p-polarized interactions. The scale length for the curves is given on the upper x-axis. The best fit of the analytic model to the experimental data is achieved for a constant expansion velocity of 24 nm ps^{-1} in all cases, which is the conversion factor between upper and lower x-axis. In the case of s-polarization, an unperturbed electron density, $N = 20$, gives the best fit to the experimental data.

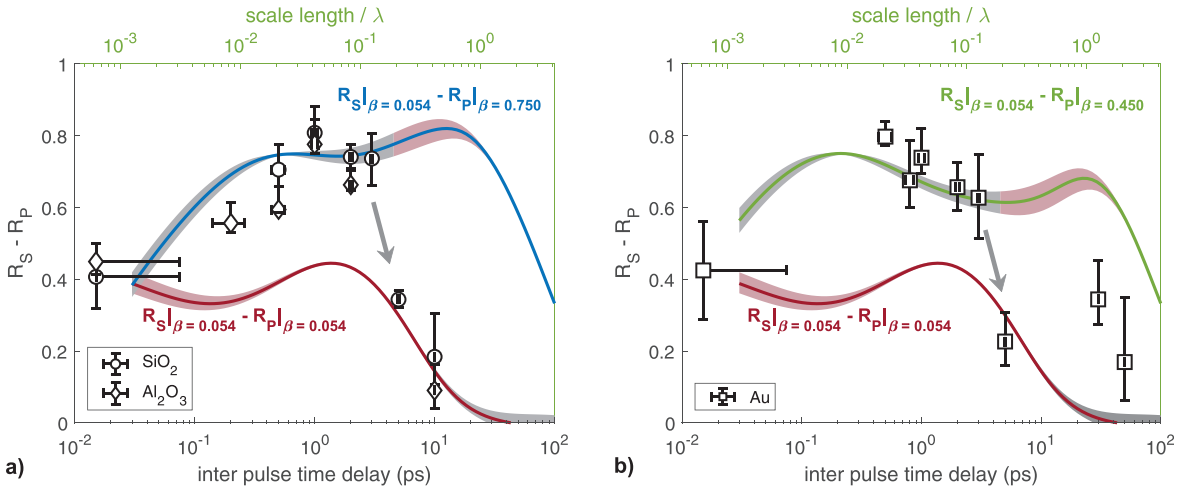

FIG. 6. [(a) and (b)] The difference in reflected energy fraction between s- and p-polarized interactions for three different collisionality ratios as calculated from the analytic model is shown by lines. This is compared to the experimentally measured values for (a) BK7 glass and sapphire, and (b) gold. (a) $\beta_P > \beta_S$, represented by the blue line, best fits the data for scale lengths less than around 125 nm, whilst for scale lengths longer than this, the red line representing $\beta_P = \beta_S$ better fits the experimental data. (b) Qualitatively the same trend is observed for gold. In both cases, the error bar in the model represents the effect of changing the collision frequency by 10% and its color is intended to guide the eye to its region of validity, gray being where the model fits the data, and red being where it does not. A summary of the best fitting parameters for the model is presented in Table I.

data show the same trends expected for p-polarized interactions as those shown in Fig. 1.

All materials also show a consistent temporal evolution of the reflected energy fraction, with all observed to have a similar reflectivity minimum at the same interpulse time delay of 1 ps. This is a material independent trend and is strong evidence for a plasma expansion dominated by a common species in each case. The most likely candidate for a common species would be protons, which is consistent with routine observations in relativistic intensity ion acceleration experiments, where protons are predominantly accelerated independent of the target material chosen. This observed material independence is our first justification for assuming, $Z^* = 1$, and, $m_i = m_p$, in the above electron temperature calculation.

The data set from interactions with beams in p-polarization is not as simple to fit to the model as the data for the s-polarization data set, as no single collision frequency describes the whole data set for all materials that were tested. We do however find that the scale length evolution is well described by the same expansion velocity as obtained from the s-polarized data. This is to say that the prepulse in both cases initiates a plasma expansion that is mutually consistent in terms of scale length evolution.

We will first describe the fitting method to the model before going on to give a physical interpretation of these results in Sec. V.

2. Temporally evolving collision frequency

In the case of matching the model to the experimentally measured p-polarization reflectivity curves, no single collision frequency appears to adequately reproduce the experimental data. However, a simple two collision frequency model appears to describe the data set for two groups of experimental data. For p-polarized interactions with short density scale lengths, an observed collision frequency $\beta_{P_{OBS}} = 0.75$ approximately fits the data, and for longer scale lengths, a smaller collision frequency of $\beta_{P_{OBS}} = 0.054$ fits the data.

Whilst Fig. 5 shows an intuitive way to fit the model to the data set as a whole, Figs. 6(a) and 6(b) show an alternative way to visualize the data set. By deducting the modeled p-polarization reflectivity at a given collision frequency, $R_P|_{\beta_P}$, from the modeled reflectivity for an s-polarized beam at another collision frequency, $R_S|_{\beta_S}$, the two trends are combined into a single trend. Similarly, the two experimentally measured data sets can be distilled from two measurements to a single measurement, $R_S - R_P$. By reducing the dimensionality of the data, it

TABLE I. A summary of the fitting parameters for the model from Fig. 6 and their observed substrate dependencies.

		Scale length vs skin depth	
		$L/\lambda < c/\omega_{pe}$	$L/\lambda > c/\omega_{pe}$
Laser polarization	s-polarization	$\beta_{S_{OBS}} = 0.054$ (substrate independent)	$\beta_{S_{OBS}} = 0.054$ (substrate independent)
	p-polarization	$\beta_{P_{OBS}} = 0.45$ (gold), $= 0.75$ (oxygen) (substrate dependent)	$\beta_{P_{OBS}} = \beta_{S_{OBS}} = 0.054$ (substrate independent)

is possible to more precisely fit the model to the data. A summary of the best fitting parameters for the model is presented in Table I.

In Fig. 6(a), this is shown for interactions with BK7 glass and sapphire. For scale lengths less than ∼125 nm, the data are best fit by differing collision frequencies, $\beta_{P_{OBS}} = 0.75 > \beta_{S_{OBS}} = 0.054$. However, for scale lengths longer than ∼125 nm, a common collision frequency is found to fit the data with, $\beta_{S_{OBS}} = \beta_{P_{OBS}} = 0.054$.

Similarly for a gold substrate, as shown in Fig. 6(b), the data are fit by $\beta_{P_{OBS}} = 0.45 > \beta_{S_{OBS}} = 0.054$ for scale lengths less than ∼125 nm and are better fit for longer scale lengths with a common collision frequency, $\beta_{S_{OBS}} = \beta_{P_{OBS}} = 0.054$.

Looking at both data sets, the transition from, $\beta_{P_{OBS}} > \beta_{S_{OBS}}$, to, $\beta_{P_{OBS}} = \beta_{S_{OBS}}$, is quasi material independent and is found to occur when the scale length of the plasma at the critical density is on the order of its skin depth, c/ω_{pe}, of 125 nm.

For absorption of p-polarized light in short density scale lengths, fitting the model to the experimental data for yield the prediction that the collisionality of the oxygen plasma should be higher than that of the gold plasma, assuming that oxygen is the dominant ion species for both BK7 (SiO_2) and sapphire (Al_2O_3). To investigate whether this should be the case, the expected collisionality of the two plasmas was calculated using the model by Eidmann *et al.*,[48] with an electron temperature of 6 eV, and the charge state of the ions was calculated using the Atzeni model.[49] This is presented in Fig. 7 and shows that a gold plasma is calculated to have a lower collisionality than an oxygen plasma under these conditions, and quantitatively also agrees well with the best fit values, where we obtain $\beta_{P_{OBS}} = 0.75$ for BK7/sapphire and $\beta_{P_{OBS}} = 0.45$ for gold.

Whilst a transition from $\beta_{P_{OBS}} > \beta_{S_{OBS}}$ to $\beta_{P_{OBS}} = \beta_{S_{OBS}}$ is most evidently observed in the data for interpulse time delays of 5–10 ps on each of the PM substrates, two outliers are observed at 30 ps and 50 ps for the gold substrate. For these shots, the near-field distribution measured from the post-PM interaction becomes distorted by intensity perturbations, as the surface quality of the PM deteriorates over time.[4]

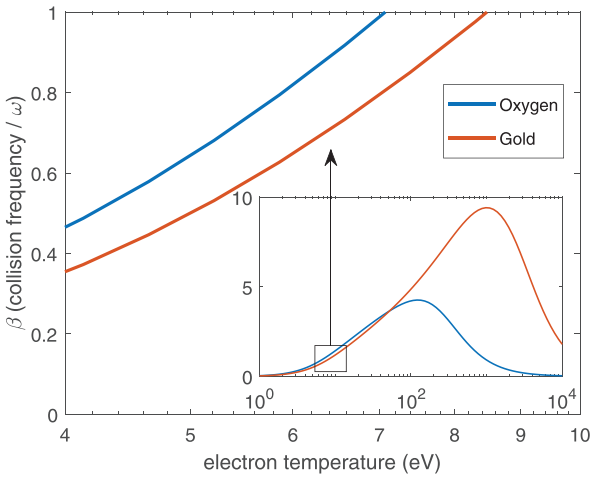

FIG. 7. The collision frequency in the bulk target material, calculated using the model by Eidmann *et al.*[48] with free electron densities based on the ionization state predicted by the More model[49] and the material densities under standard conditions.

This results in a larger error in measuring the plasma reflectivity in a sub-sampled area of the beam, contributing to a larger error and results in a larger discrepancy with the model. The data obtained from the higher-quality near-field measurements at 10-ps interpulse time delays and less therefore are objectively better quality data for comparing with the analytic model, but results from longer interpulse time delays are included here for completeness.

V. DISCUSSION

Fitting the model to the experimental data in Sec. IV shows that the temporally evolving plasma mirror reflectivity can be explained well with an evolving two collision frequency model, and our interpretation of this result follows.

For p-polarization, the absorption efficiency has two parts: η_P from Eq. (7), which a significant part of this manuscript was dedicated to formulating an analytic description for; and η_{WKB} from Eq. (5). Each of these are found here to be described by different collisional frequencies.

In the case of a long scale length, $L/\lambda \gg 1$, the mathematics here can be used to show $\eta_P \to 0$, and accordingly at large scale lengths, $\eta_{P_{TOTAL}} = \eta_{S_{TOTAL}} = \eta_{WKB}$. In this case, the collision frequency must coincide with the value obtained for s-polarization, $\beta_{WKB} = 0.054$.

On the other hand, for short scale lengths, the effective collision frequency required to reproduce the data is $\beta_{P_{OBS}} = 0.45 - 0.75$, since $L/\lambda \ll 1$; then $\eta_{WKB} \to 0$, and the main contribution to the absorption is from η_P from Eq. (7).

The p-polarized interactions are therefore found to have a material dependent collisionality for short scale length plasma, and a material independent collisionality for long scale length plasma, and this is consistent with a decoupling of two plasma species as this scale length develops. At short scale lengths, the electric field of the p-polarized laser penetrates into the high-density bulk plasma, where the bulk material properties govern the absorption efficiency of laser light, and this is observed through the differing collisionality fits for oxygen and gold plasmas.

However, for long scale lengths, the absorption efficiency of p-polarized beams is found to be independent of PM material and is found to tend toward the absorption efficiency for s-polarized beams. This is consistent with the interaction, in all cases, being with an ion species, independent of the target material choice. The probable candidate for this would be a proton plasma layer, as is routinely observed from relativistic intensity ion acceleration experiments, where protons are predominantly accelerated independent of the target material chosen.

This contaminant layer governs the expansion observed at the surface.[29,30] This can be considered similar to the end goal of the often utilized technique of tamping, to suppress the bulk expansion at the expense of the expansion of the tamping layer; the monolayers being the tamping in this analogy. This is consistent with the expansion velocity being measured to be independent of target material, as in this case, it would be dictated by the expansion velocity of protons. This is observed in the constant sound speed fit, and the scale length at which the collision frequency transitions from $\beta_{P_{OBS}} > \beta_{S_{OBS}}$ to $\beta_{P_{OBS}} = \beta_{S_{OBS}}$, being material independent.

VI. CONCLUSIONS

We have experimentally determined the plasma electron temperature, scale length, and collisionality evolution by varying laser

polarization and have measured the plasma reflectivity as a function of interpulse delay. The experimental technique in itself is simple; however, we have shown it to be particularly powerful for its sensitivity in extracting plasma parameters that are in good agreement with the predictions of models in the literature. This gives confidence that the technique can be used in future experiments and allows the picosecond evolution of these parameters to be estimated by making no prior assumptions about the plasma composition. This technique therefore provides a means of measuring sub-micron density gradients and collision frequencies in the vicinity of the critical surface, which is difficult to measure by alternative existing diagnostic techniques at solid density.

The power of this technique has led us to make novel conclusions on the nature of the plasma expansion on the picosecond timescale and sub-micron scale lengths, specifically that the laser interaction with the plasma is described by two eras: a high collisionality era where the bulk target ions play an important role in laser energy absorption, followed by a lower collisionality era, which is consistent with a hydrogen plasma expansion from surface monolayers decoupling from the bulk plasma.

This sheds new light on the kinematics of the plasma expansion at these intensities, temperatures, and timescales, which may be of relevance to field of hydrodynamic modeling, which often assume an equation of state composed of non-decoupling species, and neglect the effect due to contaminant monolayers, which we would now argue requires revision.

In previous work, PIC (Particle in Cell) modeling was used to infer that an observed PM reflectivity enhancement from 85 to 96% was due to the presence of a finite density scale length plasma of 0.1–0.3 μm on the PM surface.[4] Here, we have obtained excellent agreement, where we have measured a peak plasma mirror reflectivity of 95% for a measured plasma scale length in the region of 0.1–0.3 μm, and this work provides direct experimental evidence linking that enhanced plasma reflectivity to the presence of a density scale length.

VII. OUTLOOK

Carrying on with this work, we envisage that a relatively simple diagnostic of sub-micron plasma evolution could be installed in any experimental area, where access to a short pulse CPA (Chirped Pulse Amplification) beam exists, and has enough energy such that when the pulse duration is stretched to tens of picoseconds, it maintains an intensity of $>10^{15}$ W cm^{-2} for efficient resonant absorption.

With the stretched, chirped, pulse having a temporally varying wavelength arriving at the target $\lambda(t)$, the spectrally dependent reflectivity $R(\lambda)$, encodes information about the temporally varying reflectivity from the target $R(t)$. A similar such instrument has been demonstrated by Green *et al.* for imaging spectroscopic applications.[50] For this approach, a simultaneous s- and p-polarized measurement would be required, which could be achieved by irradiating the target with collinear, cotimed, and orthogonally polarized beams.

For measuring the preplasma scale lengths of higher intensity interactions, we calculate this technique would be adequate for the measurement of micrometer density scale lengths of mildly relativistic interactions (up to 2×10^{18} W cm^{-2}) using high contrast laser systems (10^7 at 0.5 ps).[6,51–53] Such conditions may necessarily be facilitated by PMs using current state-of-the-art technology, but as laser technology progresses using cross-beam polarization to further enhance CPA laser contrast for example, such applications should become more wideranging.

Going forward we believe this work will provide a platform for understanding of a host of plasma optic tools such as focusing PMs or reentrant cones, which have been challenging to understand or accurately model to date.

DEDICATION

This work was part of an ongoing project that the authors had the privilege of working on with our friend, colleague, and collaborator, David Neely, who sadly passed away in August 2020. Hidden between the lines of this paper are traces of several of David's most endearing and respected qualities. The diversity of authorship speaks to David's natural ability to network and establish strong international collaborations. The contributions from early career researchers and student coauthors point to David's passion for mentoring younger scientists and creating opportunities for them. The number of authors contributing from David's home institute alludes to the importance he placed on engaging and involving the community around him. Everyone who knew David admired and respected him for his passion for science, his friendship, and his generosity. He inspired the many who looked up to him and could not have done more for those around him, to ensure they were equipped for the moment and the future.

In recalling David's contributions to this research, we remember him as a down-to-earth, energizing, entertaining, and caring person, who loved performing experiments. Beyond his notorious habit of prodding a probingly insightful, "Can I ask a silly question…?," "Why don't you just…," or "Have you thought of…," this work reminds us of how privileged we were to spend time with him as a scientist and a person. We therefore feel this work is a suitable dedication to the memory of our friend, David.

ACKNOWLEDGMENTS

The authors gratefully acknowledge the assistance of the Central Laser Facility operations staff. We also gratefully acknowledge funding from EPSRC Grant Nos. EP/J003832/1, EP/K022415/1, and EP/L001357/1 and support by the Research Council of the Hochschule Emden/Leer.

This work was partially performed under the auspices of the U.S. Department of Energy by the Lawrence Livermore National Laboratory under Contract No. DE-AC52-07NA27344 and supported under DOE Early Career Grant No. SCW1651-1 and DOE FES Measurements Innovations Grant No. SCW1720 with funding support from the Laboratory Directed Research and Development Program under tracking code 21-ERD-015.

Part of the work was done in the frame of JIHT RAS state assignment of Ministry for Science and Higher Education of Russia.

A.A. and U.T. are grateful to the Deutscher Akademischer Austauschdienst (DAAD) for support by the DAAD Gastdozentenprogramm, Grant No. 57371110.

APPENDIX: EXTRA DETAILS ON THE DERIVATION OF THE SURFACE IMPEDANCE

To be concise, second-order considerations were omitted in the derivation of the surface impedance in Eq. (10), and a more through derivation is presented below.

In the case of short scale lengths ($L/\lambda < 1$), the WKB approximation fails and we therefore aim to develop a solution of (4) in the limit where the collision frequency is small, $\beta_P \ll 1$. Introducing a new variable, $\xi = x/L + N + 1$, and substituting (3) into (4), we obtain:

$$\frac{d^2H}{d\xi^2} - \frac{dH/d\xi}{\xi - i\beta_P(1+\xi)][1+i\beta_P(1+\xi)]} - \alpha H\left[\frac{\xi - i\beta_P(1+\xi)}{(1+i\beta_P(1+\xi)} + S\right] = 0, \tag{A1}$$

where $\alpha = (\omega L/c)^2$ and $S = \sin^2\theta$.

A solution of (6) and (A1) can be found by making the assumption that $\alpha \ll 1$. It should be noted that one cannot expand H in terms of α directly in (6) and (A1), since the last term, proportional to α, may become large at $\xi \to \infty$, so (6) and (A1) are solved for the edge region ($\xi \cong 1$) and in the plasma bulk ($\xi \gg 1$) separately and then matching of the expansions is performed.

When the magnetic field, H, is known, the electrical component, E_y, and the absorption efficiency of the p-polarized light in the density scale length, η_P, are given by (7) and (A2):[45]

$$E_y = i\epsilon^{-1}\alpha^{-1/2}dH/d\xi, \qquad \eta_P = 1 - |(\zeta - \cos\theta)/(\zeta + \cos\theta)|^2, \tag{A2}$$

where $\zeta = (E_y/H)|_{\xi=1}$ is the surface impedance.

Considering the region, $1 \le \xi \le N+1$, where the last term in (6) and (A1) is small compared with the other terms. Setting $\alpha = 0$, we obtain a zeroth-order approximation to the edge solution, which is valid for all values of β_P:

$$H_0 = 2D\left[\frac{i}{\beta_P^2}\arctan[\beta_P(1+\xi)] - \frac{\xi(i+\beta_P)}{\beta_P} + \frac{1}{2\beta_P^2}\ln\left[1+\beta_P^2(1+\xi)^2\right]\right] + B, \tag{A3}$$

where D and B are undefined constants. Treating β_P^2 as a small parameter in the same way as α and substituting (9) and (A4) the expansion:

$$H = H_0(\xi) + \alpha H_\alpha(\xi) + i\beta_P H_{\beta_P}(\xi) + \cdots, \tag{A4}$$

into (6) and (A1), one can obtain the following result:

$$H_0 = D\xi^2 + B, \tag{A5}$$

$$H_\alpha = B_1 - D/10 + DS/8 - B/6 + BS/4 + \xi^2(D_1 + D/6 - DS/4 + B/2 - BS/4) + (BS/2)\xi^2\ln\xi + (B/3)\xi^3 + (DS/8)\xi^4 + (D/15)\xi^5 + \xi^2\begin{cases} 0 & \xi \le 0, \\ i\pi BS/2 & \xi \ge 0, \end{cases} \tag{A6}$$

$$H_\beta = B_2 - 2D\xi + D_2\xi - (2/3)D\xi^3, \tag{A7}$$

where D_1, D_2, B_1, B_2 are constants to be defined by matching the edge and bulk solutions. The capability of the matching procedure is provided by the assumption $\alpha \ll 1$, because in this case, the edge region can overlap the bulk one. After matching, we obtain the desired values of the constants. Substituting (A5)–(A7) into the expression for ζ, we obtain the following:

$$\zeta = 2i\alpha^{-1/2}(D + \alpha D_1 + i\beta_P D_2)\cdot(D + B + \alpha(D_1 + B_1) + i\beta_P D_2)^{-1}, \tag{A8}$$

where

$$D_1, D_2, B_1, B_2, q_0, \text{ and } q_1 \tag{A9}$$

are constants to be defined by matching the edge and bulk solutions. The capability of the matching procedure is provided by the assumption $\alpha \ll 1$, because in this case, the edge region can overlap the bulk one.

$$D = -(3^{1/3}/4)\Gamma(1/3)\alpha^{2/3},$$

$$D_1 = -\frac{B(1+i\pi S)}{2} - S\left[\frac{q_0}{6^{1/3}}\Gamma(2/3) + \frac{\Gamma(2/3)(\gamma + \ln(2\alpha^{1/2})/3)}{2\cdot 3^{1/3}}\right],$$

$$D_2 = \frac{\alpha^{1/3}(3\Gamma(1/3)/40 + q_1/3\cdot 2^{2/3})}{/}\Gamma(2/3),$$

$$B = (3^{3/2}/2)\Gamma(2/3),$$

$$B_1 = \frac{B(1-3S/2)}{6},$$

where

$$q_0 = \int_0^\infty t^{1/3}\left[K(2/3)^2(t) - \Gamma^2(2/3)(2t^2)^{(-2/3)}\exp(-t)\right]dt \cong -0.31,$$

$$q_1 = \int_0^\infty t^{-1/3}\left[K(2/3)^2(t) - \Gamma^2(2/3)(2t^2)^{(-2/3)}\right]dt \cong -4.29, \tag{A10}$$

where K is the MacDonald function.

Relation (10) can be approximated by

$$\zeta \approx -1.38i\cdot\alpha^{1/6}[1 - \alpha^{1/3}S] + \pi\alpha^{1/2}S + 0.38\beta_P\alpha^{-1/6}, \tag{A11}$$

where the real terms are responsible for resonant and collisional parts of the total absorption efficiency. The absence of the angular dependence in the last term of (12) and (A11) implies the equality of collisional absorption efficiency for the s- and p-polarized waves in the considered approximation.

DATA AVAILABILITY

The data that support the findings of this study are available from the corresponding author upon reasonable request.

REFERENCES

[1]C. Ziener, P. S. Foster, E. J. Divall, C. J. Hooker, M. H. R. Hutchinson, A. J. Langley, and D. Neely, J. Appl. Phys. **93**, 768 (2003).
[2]B. Dromey, S. Kar, and M. Zepf, Rev. Sci. Instrum. **75**, 645 (2004).
[3]G. Doumy, F. Quere, O. Gobert, M. Perdrix, P. Martin, P. Audebert, J. C. Gauthier, J.-P. Geindre, and T. Wittmann, Phys. Rev. E **69**, 026402 (2004).
[4]G. G. Scott, V. Bagnoud, C. Brabetz, R. J. Clarke, J. S. Green, R. I. Heathcote, H. W. Powell, B. Zielbauer, T. D. Arber, P. McKenna, and D. Neely, New J. Phys. **17**, 033027 (2015).
[5]S. K. Mishra, A. Andreev, and M. P. Kalashinikov, Opt. Express **25**, 11637 (2017).

[6]S. Inoue, K. Maeda, S. Tokita, K. Mori, K. Teramoto, M. Hashida, and S. Sakabe, Appl. Opt. **55**, 5647 (2016).
[7]X. Ge, X. Yuan, Y. Fang, W. Wei, S. Yang, F. Liu, M. Chen, L. Zhao, Z. Sheng, and J. Zhang, Chin. Opt. Lett. **16**, 103202 (2018), https://www.osapublishing.org/col/abstract.cfm?uri=col-16-10-103202
[8]A. Borot, D. Douillet, G. Iaquaniello, T. Lefrou, P. Audebert, J.-P. Geindre, and R. Lopez-Martens, Rev. Sci. Instrum. **85**, 013104 (2014).
[9]P. L. Poole, A. Krygier, G. E. Cochran, P. S. Foster, G. G. Scott, L. A. Wilson, J. Bailey, N. Bourgeois, C. Hernandez-Gomez, D. Neely, P. P. Rajeev, R. R. Freeman, and D. W. Schumacher, Sci. Rep. **6**, 32041 (2016).
[10]B. H. Shaw, S. Steinke, J. van Tilborg, and W. P. Leemans, Phys. Plasmas **23**, 063118 (2016).
[11]M. Speicher, D. Haffa, M. A. O. Haug, J. Bin, Y. Gao, J. Hartmann, P. Hilz, C. Kreuzer, F. H. Lindner, T. M. Ostermayr, T. F. Rosch, R. Yang, and J. Schreiber, J. Phys.: Conf. Ser. **1079**, 012002 (2016).
[12]S. Steinke, J. van Tilborg, C. Benedetti, C. G. R. Geddes, C. B. Schroeder, J. Daniels, K. K. Swanson, A. J. Gonsalves, K. Nakamura, N. H. Matlis, B. H. Shaw, E. Esarey, and W. P. Leemans, Nature **530**, 190 (2016).
[13]M. Nakatsutsumi, A. Kon, S. Buffechoux, P. Audebert, J. Fuchs, and R. Kodama, Opt. Lett. **35**, 2314 (2010).
[14]R. Wilson, M. King, R. J. Gray, D. C. Carroll, R. J. Dance, C. Armstrong, S. J. Hawkes, R. J. Clarke, D. J. Robertson, D. Neely, and P. McKenna, Phys. Plasmas **23**, 03310 (2016).
[15]R. Wilson, M. King, R. J. Gray, D. C. Carroll, R. J. Dance, N. M. H. Butler, C. Armstrong, S. J. Hawkes, R. J. Clarke, D. J. Robertson, C. Bourgenot, D. Neely, and P. McKenna, Quantum Beam Sci. **2**, 1 (2018).
[16]H. Tsai, X. Wang, J. M. Shaw, Z. Li, A. V. Arefiev, X. Zhang, R. Zgadzaj, W. Henderson, V. Khudik, G. Shvets, and M. C. Downer, Phys. Plasmas **22**, 023106 (2015).
[17]Z. Y. Chen and A. Pukhov, Nat. Commun. **7**, 12515 (2016).
[18]M. Thevenet, A. Leblanc, S. Kahaly, H. Vincenti, A. Vernier, F. Quere, and J. Faure, Nat. Phys. **12**, 355 (2016).
[19]A. Morace, S. Kojima, Y. Arikawa, S. Fujioka, A. Yogo, S. Tosaki, S. Sakata, Y. Abe, S. H. Lee, K. Matsuo, A. Sagisaka, K. Kondo, A. S. Pirozhkov, T. Norimatsu, T. Jitsuno, N. Miyanaga, H. Shiraga, M. Nakai, H. Nishimura, and H. Azechi, Nucl. Fusion **57**, 126018 (2017).
[20]L. Obst, J. Metzkes-Ng, S. Bock, G. E. Cochran, T. E. Cowan, T. Oksenhendler, P. L. Poole, I. Prencipe, M. Rehwald, C. Rodel, H.-P. Schlenvoigt, U. Schramm, D. W. Schumacher, T. Ziegler, and K. Zeil, Plasma Phys. Controlled Fusion **60**, 054007 (2018).
[21]M. Zepf, G. D. Tsakiris, G. Pretzler, I. Watts, D. M. Chambers, P. A. Norreys, U. Andiel, A. E. Dangor, K. Eidmann, C. Gahn, A. Machacek, J. S. Wark, and K. Witte, Phys. Rev. E **58**, R5253 (1998).
[22]U. Teubner, K. Eidmann, U. Wagner, U. Andiel, F. Pisani, G. D. Tsakiris, K. Witte, J. Meyer-ter-Vehn, T. Schlegel, and E. Forster, Phys. Rev. Lett. **92**, 185001 (2004).
[23]U. Teubner and P. Gibbon, Rev. Mod. Phys. **81**, 445 (2009).
[24]C. Rödel, J. Bierbach, M. Yeung, T. Hahn, B. Dromey, S. Herzer, S. Fuchs, A. G. Pour, E. Eckner, M. Behmke, M. Cerchez, O. Jackel, D. Hemmers, T. Toncian, M. C. Kaluza, A. Belyanin, G. Pretzler, O. Willi, A. Pukhov, M. Zepf, and G. G. Paulus, Phys. Rev. Lett. **109**, 125002 (2012).
[25]M. J. V. Streeter, P. S. Foster, F. H. Cameron, M. Borghesi, C. Brenner, D. C. Carroll, E. Divall, N. P. Dover, B. Dromey, P. Gallegos, J. S. Green, S. Hawkes, C. J. Hooker, S. Kar, P. McKenna, S. R. Nagel, Z. Najmudin, C. A. J. Palmer, R. Prasad, K. E. Quinn, P. P. Rajeev, A. P. L. Robinson, L. Romagnan, J. Schreiber, C. Spindloe, S. Ter-Avetisyan, O. Tresca, M. Zepf, and D. Neely, New J. Phys. **13**, 023041 (2011).
[26]D. Neely, P. Foster, A. Robinson, F. Lindau, O. Lundh, A. Persson, C.-G. Wahlström, and P. McKenna, Appl. Phys. Lett. **89**, 021502 (2006).
[27]P. McKenna, D. C. Carroll, O. Lundh, F. Nürnberg, K. Markey, S. Bandyopadhya, D. Batani, R. G. Evans, R. Jafer, S. Kar, D. Neely, D. Pepler, M. N. Quinn, R. Redaelli, M. Roth, C.-G. Wahlström, X. H. Yuan, and M. Zepf, Laser Part. Beams **26**, 591 (2008).
[28]R. J. Gray, D. C. Carroll, X. H. Yuan, C. M. Brenner, M. Burza, M. Coury, K. L. Lancaster, X. X. Lin, Y. T. Li, D. Neely, M. N. Quinn, O. Tresca, C.-G. Wahlstrom, and P. McKenna, New J. Phys. **16**, 113075 (2014).
[29]R. A. Loch, T. Ceccotti, F. Quere, H. George, G. Bonnaud, F. Réau, P. D'Oliveira, M. J. H. Luttikhof, F. Bijkerk, K.-J. Boller, G. Blaclard, and P. Combis, Phys. Plasmas **23**, 093117 (2016).
[30]G. G. Scott, D. C. Carroll, S. Astbury, R. J. Clarke, C. Hernandez-Gomez, M. King, A. Alejo, I. Y. Arteaga, R. J. Dance, A. Higginson, S. Hook, G. Liao, H. Liu, S. R. Mirfayzi, D. R. Rusby, M. P. Selwood, C. Spindloe, M. K. Tolley, F. Wagner, E. Zemaityte, M. Borghesi, S. Kar, Y. Li, M. Roth, P. McKenna, and D. Neely, Phys. Rev. Lett. **120**, 204801 (2018).
[31]U. Teubner, G. Kuhnle, and F. P. Schafer, Appl. Phys. Lett. **59**, 2672 (1991).
[32]U. Teubner, C. Wulker, and W. Theobald, Phys. Plasmas **2**, 972 (1995).
[33]W. Lu, M. Nicoul, U. Shymanovich, A. Tarasevitch, P. Zhou, K. Sokolowski-Tinten, D. von der Linde, M. Masek, P. Gibbon, and U. Teubner, Phys. Rev. E **80**, 026404 (2009).
[34]Y. Sentoku and A. J. Kemp, J. Comput. Phys. **227**, 6846 (2008).
[35]G. G. Scott, C. M. Brenner, V. Bagnoud, R. J. Clarke, B. Gonzalez-Izquierdo, J. S. Green, R. I. Heathcote, H. W. Powell, D. R. Rusby, B. Zielbauer, P. McKenna, and D. Neely, New J. Phys. **19**, 043010 (2017).
[36]S. Kahaly, S. Monchoce, H. Vincenti, T. Dzelzainis, B. Dromey, M. Zepf, P. Martin, and F. Quere, Phys. Rev. Lett. **110**, 175001 (2013).
[37]M. Bocoum, F. Bohle, A. Vernier, A. Jullien, J. Faure, and R. Lopez-Martens, Opt. Lett. **40**, 3009 (2015).
[38]A. Leblanc, S. Monchoce, H. Vincenti, S. Kahaly, J.-L. Vay, and F. Quere, Phys. Rev. Lett. **119**, 155001 (2017).
[39]O. L. Landen, D. G. Stearns, and E. M. Campbell, Phys. Rev. Lett. **63**, 1475 (1989).
[40]D. C. Carroll, M. Coury, G. Scott, P. McKenna, M. J. V. Streeter, H. Nakamura, Z. Najmudin, F. Fiorini, S. Green, J. S. Green, P. Foster, R. Heathcote, K. Poder, D. Symes, R. J. Clarke, R. Pattahil, and D. Neely (CLF, 2011).
[41]Y. Cai, W. Wang, C. Xia, J. Liua, L. Liu, C. Wang, Y. Xu, Y. Leng, R. Li, and Z. Xu, Phys. Plasmas **16**, 103104 (2009).
[42]V. L. Ginzburg, *Propagation of Electromagnetic Waves in Plasma* (Gordon & Breach Science Publishers Ltd, 1961).
[43]W. L. Kruer, *The Physics of Laser Plasma Interactions* (Addison-Wesley, New York, 1988).
[44]P. Gibbon, *Short Pulse Laser Interactions with Matter: An Introduction* (World Scientific, London, 2005).
[45]A. A. Andreev and K. Y. Platonov, Plasma Phys. Rep. **24**(1), 26 (1998), https://inis.iaea.org/search/search.aspx?orig_q=RN:35015336
[46]J.-C. Kieffer, J.-P. M. S. Belair, M. Chaker, P. Audebert, H. Pepin, P. Maine, D. Strickland, P. Bado, and G. Mourou, J. Quantum Electron. **25**, 2639 (1989), https://ieeexplore.ieee.org/abstract/document/40652
[47]A. A. Andreev, J. Limpouch, A. B. Iskakov, and H. Nakano, Phys. Rev. E **65**, 026403 (2002).
[48]K. Eidmann, J. Meyer-Ter-Vehn, T. Schlegel, and S. Huller, Phys. Rev. E **62**, 1202 (2000).
[49]S. Atzeni, *The Physics of Inertial Fusion: Beam Plasma Interaction, Hydrodynamics, Hot Dense Matters* (Oxford University Press, Oxford, 2004).
[50]J. S. Green, N. Booth, R. J. Dance, R. J. Gray, D. A. MacLellan, A. Marshall, P. McKenna, C. D. Murphy, C. P. Ridgers, A. P. L. Robinson, D. Rusby, R. H. H. Scott, and L. Wilson, Sci. Rep. **8**, 4525 (2018).
[51]S. C. Wilks, W. L. Kruer, M. Tabak, and A. B. Langdon, Phys. Rev. Lett. **69**, 1383 (1992).
[52]V. Bagnoud and F. Wagner, High Power Laser Sci. Eng. **4**, e39 (2016).
[53]S. J. Hawkes, private communication (2020).